 https://doi.org/10.3311/PPch.40001

Periodica Polytechnica Chemical Engineering, 69(2), pp. 204–218, 2025

Optimizing Semiconductor-insulator-semiconductor Heterojunction Engineering Performance in a Novel High-efficiency Solar Cell Structure

Ahmed Bouriche[1,2], Charazade-Elj Benouis[1,2], Mostefa Benhaliliba[1,2*], Keltoum Dris[1,2,3]

[1] Films and Devices Fabrication and Characterization-Applications (FDFCA) Research Group, University of Science and Technology of Oran Mohamed-Boudiaf (USTOMB), P. O. B. 1505, 31000 Oran, Algeria
[2] Faculty of Physics, University of Science and Technology of Oran Mohamed-Boudiaf (USTOMB), P. O. B. 1505, 31000 Oran, Algeria
[3] Laboratoire d'études Physiques des matériaux (LEPM), Université des Sciences et de la Technologie d'Oran Mohamed-Boudiaf (USTOMB), BP 1505, 31000 Oran, Algérie
* Corresponding author, e-mail: mostefa.benhaliliba@univ-usto.dz

Received: 26 January 2025, Accepted: 22 May 2025, Published online: 24 June 2025

Abstract

In this study, we introduce and optimize a novel semiconductor-insulator-semiconductor (SIS) solar cell using SCAPS-1D simulations. The Pt/Si/TiO_2/ZnSe/ fluorine-doped tin oxide (FTO), structure employs Pt and FTO as back/front contacts. TiO_2 serves as a critical insulating layer between p-Si and n-ZnSe, enhancing electrical isolation while boosting stability and efficiency through reduced recombination and improved charge transport. Results demonstrate TiO_2 as an insulating material significantly improves the fill factor (FF) and power conversion efficiency (PCE) of the device, compared to conventional structures. Key optimized parameters include: Si 1300 nm, ZnSe 100 nm, and TiO_2 insulating layer to 10 nm; defect densities of 10^{15} cm^{-3} for both Si and ZnSe, and 10^{12} cm^{-3} for the interfaces. This optimized cell demonstrates the following performance results: a V_{OC} of 0.84 V, a J_{SC} of 42.09 mA cm^{-2}, an FF of 86.42%, and a PCE of 30.65%. These results were achieved under standard test conditions (AM1.5G, temperature of 300 K). Our simulations focus on enhancing electrical parameters, particularly efficiency. This study will provide valuable parameters for any future experimental work on SIS solar cells.

Keywords

SIS solar cell, power conversion efficiency, TiO_2, ZnSe, optimization, SCAPS-1D

1 Introduction

For several decades, climate change and global warming have presented significant challenges. These issues have perpetuated serious economic, social, and environmental problems, with human health being particularly at risk. Experts contend that human activities are detrimental to the environment [1, 2].

The primary sources of energy around the globe are fossil fuels, including oil, natural gas, and coal. This reliance greatly contributes to greenhouse gas emissions, which subsequently result because greenhouse gas emissions in global warming. Among renewable energy options, solar energy is particularly advantageous and can be harnessed through photovoltaic or thermal methods [3, 4].

Solar energy is globally abundant in potential, though its accessibility varies significantly by geography, climate, infrastructure, and socioeconomic factors. The sun generates an enormous amount of energy, making it a nearly infinite resource. In contrast to finite fossil fuels that are depleting, solar power provides a dependable and sustainable energy option. Furthermore, solar energy can be harnessed in almost any location on Earth that receives sunlight. This broad geographical availability allows solar energy to reach many areas, including remote and off-grid regions where traditional power systems may be difficult and expensive to establish. By utilizing solar energy, we can significantly reduce our carbon emissions and contribute to combating climate change. It also helps decrease air and water pollution, protecting both the environment and public health [5].

In 1883, Fritts [6] introduced an unconventional solar cell that exhibited very poor efficiency, approximately 1%.

Cite this article as: Bouriche, A., Benouis, C.-E., Benhaliliba, M., Dris, D. "Optimizing Semiconductor-insulator-semiconductor Heterojunction Engineering Performance in a Novel High-efficiency Solar Cell Structure", Periodica Polytechnica Chemical Engineering, 69(2), pp. 204–218, 2025.
https://doi.org/10.3311/PPch.40001

This design replaced the traditional silicon homo-junction with a metal-semiconductor Schottky junction [6].

In the subsequent years, researchers made substantial strides in enhancing the efficiency of Schottky barrier solar cells. This progress was achieved by optimizing the thickness of the metal layer and incorporating an insulating layer between the metal and the semiconductor. These modifications help minimize crystal defects at the junction interface, resulting in a significant improvement in performance [7, 8].

Semiconductor-insulator-semiconductor (SIS) solar cells are gaining increasing interest due to their potential to enhance energy efficiency and simplify manufacturing processes.

First introduced in the 1970s, this concept was explored through studies on indium tin oxide (ITO)/p-Si cells, highlighting the critical role of the ITO-silicon interface in maximizing conversion efficiency [9]. Since then, significant advancements have been made, particularly with the integration of metal oxides as tunneling barriers in composite structures. For instance, Bethge et al. [10] demonstrated the efficiency of metal oxide films deposited via atomic layer deposition (ALD), such as Al_2O_3, ZrO_2, and La_2O_3, in SIS structures. They reported that the rare-earth oxide La_2O_3 enabled a conversion efficiency of 8% on a 1.4 cm^2 cell [10]. However, certain oxides exhibit undesirable chemical reactivity, affecting device performance. Kobayashi et al. [11] also showed enhanced performance in Si/ITO cells with the addition of a silicon oxide layer at the interface, which facilitated charge carrier transport via tunneling.

More recently, Dasgupta et al. [12] developed a model for an SIS cell with an interdigitated back contact (IBC). They demonstrated that a thin thermally deposited silicon oxide layer between ZnO and Si reduced interface defects and improved overall cell performance [12]. Additionally, the integration of ZnO formed an efficient p-n or heterojunction, which improved charge transport and reduced losses, thereby boosting conversion efficiency [13, 14]. In another study, Dasgupta et al. [15] explored an ITO-Al_2O_3-Si cell, where an Al_2O_3 layer served as a tunneling barrier, reducing carrier recombination while enhancing conductivity. Furthermore, the integration of nanoparticles in solar cells has opened new possibilities. Shameli et al. [16] investigated thin-film solar cells incorporating silicon nanospheres for light trapping and confinement. This approach increased light absorption and photogenerated current, achieving up to three times the performance of conventional cells [16].

In this study, we propose a novel SIS architecture: Pt/p-Si/TiO_2/n-ZnSe/fluorine-doped tin oxide (FTO), incorporating TiO_2 as the tunneling barrier. Although TiO_2 is a semiconductor material, it is employed here as an insulating layer due to its specific properties [17]. With its wide bandgap (~3.2 eV), TiO_2 acts as an energy barrier, facilitating effective carrier transport through tunneling while blocking undesirable recombination. Moreover, its passivation properties reduce surface states and interface defects, thereby minimizing carrier losses. Compared to conventional oxides like SiO_2 or Al_2O_3, TiO_2 offers better chemical stability and increased compatibility with modern deposition techniques, ensuring a stable and high-performance interface [18–20]. This structure strategically combines materials with complementary properties. Pt is chosen as the back contact for its chemical stability and favorable energy level alignment with p-Si, ensuring efficient hole extraction. The p-type silicon acts as the primary absorber due to its indirect bandgap of 1.12 eV, making it ideal for capturing a wide spectrum of solar energy [21, 22]. The n-type zinc selenide serves as the electron transport layer because of its direct bandgap of 2.81 eV and high electron mobility, both of which improve carrier collection efficiency [23, 24].

FTO functions as the transparent front contact [23, 25]. In a recent study, El-Naggar et al. [26] utilizes FTO as the transparent front contact in a simulated $BaZrS_3$/CuO heterojunction solar cell. FTO's high electrical conductivity and superior optical transparency maximize light transmission into the cell's active layers, enhancing photon absorption and minimizing optical/electrical losses at the front interface. These properties improve charge collection efficiency and overall performance by reducing resistive losses and ensuring uniform illumination, leading to optimized solar cell functionality [26]. The structure of this cell and the associated band diagram are presented in Fig. 1.

The primary objective of this research is to enhance the performance of SIS cells by optimizing the Pt/p-Si/TiO_2/n-ZnSe/FTO configuration. Our strategy aims to improve light absorption, minimize carrier recombination, and promote efficient charge extraction. We utilize the SCAPS-1D simulator [27] to fine-tune key parameters, such as layer thickness, defect densities in the p-Si, TiO_2, and n-ZnSe layers, as well as defect densities at the interfaces. This study will evaluate recombination rates and examine the conduction and valence band structures. Additionally, we will explore the impact of temperature. The results of this research are expected to provide a solid

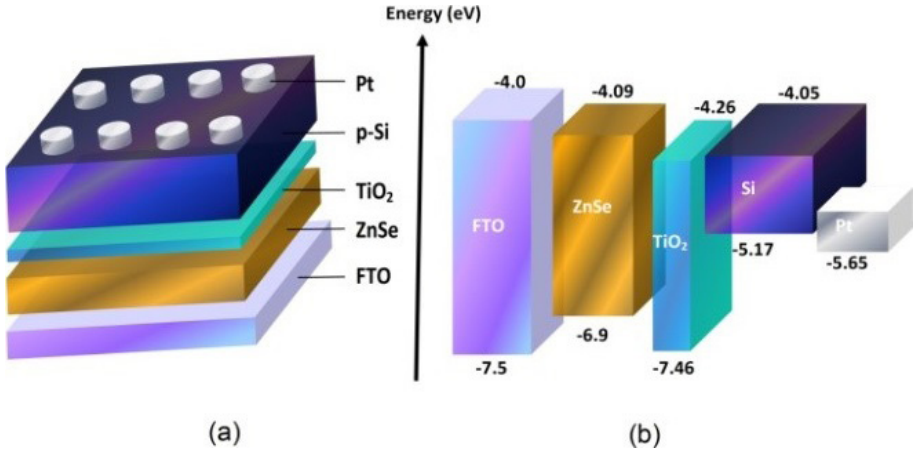

Fig. 1 (a) The structure of Pt/Si/TiO_2/ZnSe/FTO, (b) The energy band diagram

foundation for experimental progress and the development of high-performance SIS cells.

2 Parameters and simulation software

In this study, we employed the SCAPS-1D (Solar Cell Capacitance Simulator in 1 Dimension) software [27], a sophisticated tool specifically created for simulating the performance of solar cells. Developed by the University of Ghent, SCAPS-1D allows for the study of the optoelectronic behavior of multilayer photovoltaic devices by solving the fundamental semiconductor equations in a one-dimensional structure [17, 26, 28–31].

The performance of the solar cells simulated in SCAPS-1D is evaluated by solving the following three fundamental equations.

2.1 Poisson equation

The Poisson equation describes the distribution of the electric potential $V(x)$ in a semiconductor, as a function of the free carrier densities (electrons and holes), dopants, and fixed charges [32]:

$$\frac{\partial}{\partial x}\left[-\varepsilon(x)\frac{\partial V}{\partial x}\right] = q\left[p(x)-n(x)+N_D^+(x)-N_A^-(x)+p_t(x)-n_t(x)\right], \quad (1)$$

where

- $\varepsilon(x)$: permittivity of the material,
- $p(x)$, $n(x)$: concentrations of holes and free electrons, respectively,
- $N_D^+(x)$, $N_A^-(x)$: concentrations of ionized donors and acceptors,
- $p_t(x)$, $n_t(x)$: concentrations of hole and electron traps,
- q: elementary charge.

2.2 Hole continuity equation

The hole continuity equation describes the temporal evolution of the hole density $p_t(x)$, in terms of hole generation and recombination, as well as carrier transport [25, 32]:

$$\frac{\partial p}{\partial t} = \frac{1}{q}\frac{\partial J_P}{\partial x} + G_P - R_P, \quad (2)$$

where:

- J_P: hole current density,
- G_P: hole generation rate,
- R_P: hole recombination rate.

2.3 Electron continuity equation

The electron continuity equation describes the evolution of the electron density $n_t(x)$, taking into account the generation, recombination, and transport of electrons [25, 32]:

$$\frac{\partial n}{\partial t} = \frac{1}{q}\frac{\partial J_n}{\partial x} + G_n - R_n, \quad (3)$$

where:

- J_n: electron current density,
- G_n: electron generation rate,
- R_n: electron recombination rate.

2.4 Hole and electron current density

The hole and electron currents are modeled by the carrier transport relations, which include carrier mobility and the diffusion term:

- for holes [25]

$$J_P = qp\mu_p E + D_p\frac{dp}{dx} \quad (4)$$

- for electrons [23]

$$J_n = qp\mu_n E + D_n\frac{dn}{dx}, \quad (5)$$

where:

- μ_p, μ_n: mobilities of holes and electrons,
- D_p, D_n: diffusion coefficients for holes and electrons,
- E: electric field.

2.5 Steady-state conditions

Under the assumption of steady-state conditions (where $\partial n/\partial t = 0$ and $\partial p/\partial t = 0$), the electron and hole continuity equations simplify to

- for electrons [25, 33]

$$\frac{1}{q}\frac{\partial J_n}{\partial x} = -G_n(x,t) + R_n(x,t) \tag{6}$$

- for holes [23, 30]

$$\frac{1}{q}\frac{\partial J_p}{\partial x} = -G_p(x,t) + R_p(x,t). \tag{7}$$

2.6 Complete electron and hole current equations in steady-state

By substituting the expressions for J_p and J_n into the continuity equations, relations for the variations in the electric field and carrier concentrations within the device are obtained:

- for electrons [25, 33]

$$\mu_n \frac{dn}{dx} + D_n \frac{\partial^2 n}{\partial x^2} = -G_n(x) + R_n(x) \tag{8}$$

- for holes [25, 33]

$$\frac{dE}{dx} + \mu_p \frac{dp}{dx} + D_p \frac{\partial^2 p}{\partial x^2} = -G_p(x) + R_p(x). \tag{9}$$

The simulations were performed using SCAPS-1D software (version 3.3.10) [27], with the input parameters detailed in Tables 1 and 2. The analysis was conducted under standard test conditions, which include an Air Mass 1.5 Global (AM1.5G) solar spectrum, an ambient temperature of 300 K, and a power density of 1000 W/m^2. These parameters enable a consistent and realistic assessment of solar cell performance [34].

3 Results and discussion

3.1 Optimization of the silicon layer thickness

The absorber layer is crucial for the efficiency of SIS solar cells because it directly participates in photon absorption and the generation of electron-hole pairs, both of which are essential for photovoltaic conversion [35, 36].

The thickness of this layer is vital for the cell's efficiency, influencing the generation, lifespan, and diffusion length of charge carriers. An ideal absorber layer thickness improves photon absorption and minimizes losses due to charge carrier recombination. If the layer is too thin, it may not capture enough light, while excessively thick layers can lead to increased recombination and reduced overall cell performance [37].

In this section, we explored the impact of the absorber layer thickness (Si) on the cell's output parameters, varying the thickness from 100 to 1900 nm. The results are illustrated in Fig. 2. Modifying the thickness of the p-Si layer in the Pt/p-Si/TiO_2/n-ZnSe/FTO structure significantly boosts performance, reaching its peak at a thickness of 1300 nm. As the thickness increases, the short-circuit current density (J_{sc}) rises from 20.91 to 42.52 mA cm^{-2},

Table 1 Material parameters used in the cell simulation

Parameters	FTO	ZnSe	TiO_2	Si
Thickness (nm)	100	100	10	500
Band gap (eV)	3.5	2.81	3.2	1.12
Electron affinity (eV)	4.0	4.09	4.26	4.05
Dielectric permittivity	9.0	8.6	9	11.9
CB effective density of states (cm^{-3})	2.2×10^{18}	2.2×10^{18}	2×10^{18}	2.8×10^{19}
VB effective density of states (cm^{-3})	1.8×10^{19}	1.9×10^{19}	1.8×10^{19}	2.65×10^{19}
Electron thermal velocity (cm s^{-1})	1.0×10^{7}	1.0×10^{7}	1.0×10^{7}	1.0×10^{7}
Hole thermal velocity (cm s^{-1})	1.0×10^{7}	1.0×10^{7}	1.0×10^{7}	1.0×10^{7}
Electron mobility (cm^2 V^{-1} s^{-1})	20	400	20	1.45×10^{3}
Hole mobility (cm^2 V^{-1} s^{-1})	10	110	10	5.0×10^{2}
Shallow uniform donor density N_D (cm^{-3})	2×10^{19}	1.0×10^{21}	1.0×10^{16}	0
Shallow uniform acceptor density N_A (cm^{-3})	0	0	1.0×10^{16}	1.0×10^{20}
N_t (cm^{-3}) total	1.0×10^{16}	1.0×10^{14}	1.0×10^{15}	1.0×10^{14}
Reference	[23, 25]	[23, 24]	[17]	[21, 22]

CB: conduction band, VB: valence band

Table 2 The input parameters for the Si/TiO_2; TiO_2/ZnSe and ZnSe/FTO interfaces

Interface layer	Si/TiO_2	TiO_2/ZnSe	ZnSe/FTO
Type of defect	neutral	neutral	neutral
Electrons capture cross-section (cm^2)	1.0×10^{-19}	1.0×10^{-19}	1.0×10^{-19}
Hole capture cross-section (cm^2)	1.0×10^{-19}	1.0×10^{-19}	1.0×10^{-19}
Energy distribution	single	single	single
Defect energy level reference (E_t)	above the highest EV	above the highest EV	above the highest EV
Energy level related to reference (eV)	0.6	0.6	0.6
Total density integrated over all energies (cm^{-3})	1.0×10^{10}	1.0×10^{10}	1.0×10^{10}

EV: energy valence

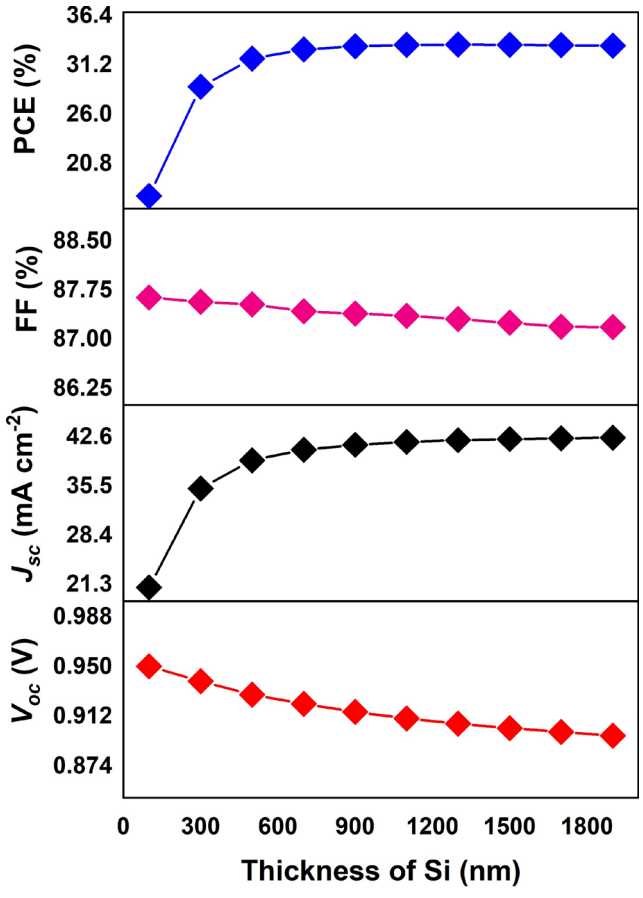

Fig. 2 The effect of silicon layer thickness on photovoltaic parameters

which is attributed to better photon absorption. In contrast, the open-circuit voltage (V_{oc}) slightly decreases from 0.95 V to 0.897 V, primarily due to increased recombination within the p-Si layer. The power conversion efficiency (PCE) reaches its maximum of 33.37% at 1300 nm before declining, indicating optimal light absorption. This pattern is associated with improved absorption of longer-wavelength photons as the thickness grows. Initially, the enhancements in J_{sc}, V_{oc}, and PCE are due to the increased generation of photocarriers [38].

To better understand how the thickness of the p-Si layer affects the device's internal mechanisms, we investigated the correlation between thickness (spanning from 100 to 1900 nm) and impedance. The results are presented in Fig. 3. The changes in the arcs of the Nyquist plots at different thicknesses show an increase in both Z' and Z'' values, indicating an improvement in internal resistances. This improvement is associated with a higher generation of charge carriers in thicker layers, along with better light absorption.

The impedance arcs demonstrate that the best performance occurs at a thickness of 1300 nm. At this thickness, there is an optimal balance between reduced recombination losses and improved charge collection, resulting in the highest PCE values. However, the continued increase in impedance beyond 1300 nm indicates a rise in recombination and a decline in charge carrier transport efficiency, ultimately leading to a decrease in PCE. The selected optimal thickness for the silicon absorber layer is 1300 nm. This thickness results in a V_{oc} of 0.907 V, a J_{sc} of 42.16 mA cm^{-2}, a fill factor (FF) of 87.31%, and a PCE of 33.37%.

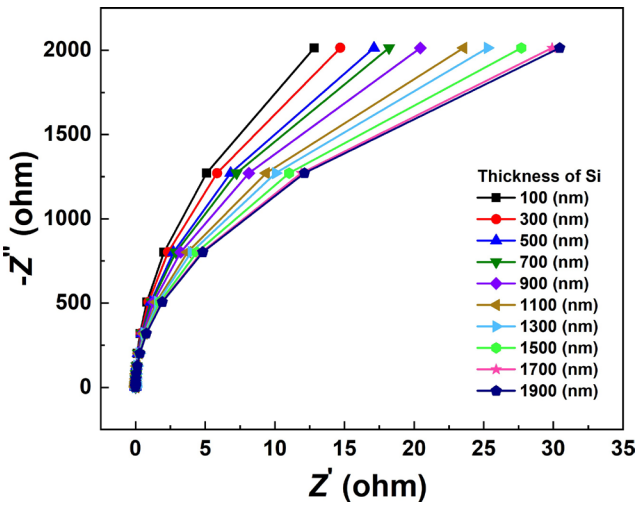

Fig. 3 Nyquist plot showing the evolution of impedance as a function of silicon thickness

3.2 Optimization of the zinc selenide layer thickness

Optimizing the thickness of the ZnSe layer is crucial for efficient electron transport and the absorption of incoming photons [39]. To evaluate how the thickness of this layer influences our solar cell, we varied it from 100 to 700 nm, and the results are shown in Fig. 4.

At a thickness of 100 nm, the cell achieves its optimal performance, boasting a PCE of 33.37%, a remarkable J_{sc} of 42.16 mA cm^{-2}, and a stable FF of 87.31%. This reflects efficient carrier collection with minimal losses due to recombination or absorption in the ZnSe layer. However, as the thickness of the ZnSe layer increases, both J_{sc} and efficiency experience a gradual decline, with J_{sc} decreasing from 42.16 to 40.47 mA cm^{-2} and PCE falling from 33.37% to 31.99%.

The reduction can be attributed to improved light absorption in the ZnSe layer, which limits the amount of light that reaches the p-Si layer, the main area for carrier generation. Additionally, increasing the thickness of the ZnSe layer may lead to higher recombination losses; however, these losses remain relatively minor, as evidenced by the minimal variation in V_{oc} [40]. Nyquist plots (Fig. 5) clearly illustrate this trend, showing an increase in resistance coupled with a decrease in charge transport efficiency. The ideal thickness for the n-ZnSe layer was found to be 100 nm, resulting in a V_{oc} of 0.907 V, a J_{sc} of 42.16 mA cm^{-2}, an FF of 87.31%, and a PCE of 33.37%.

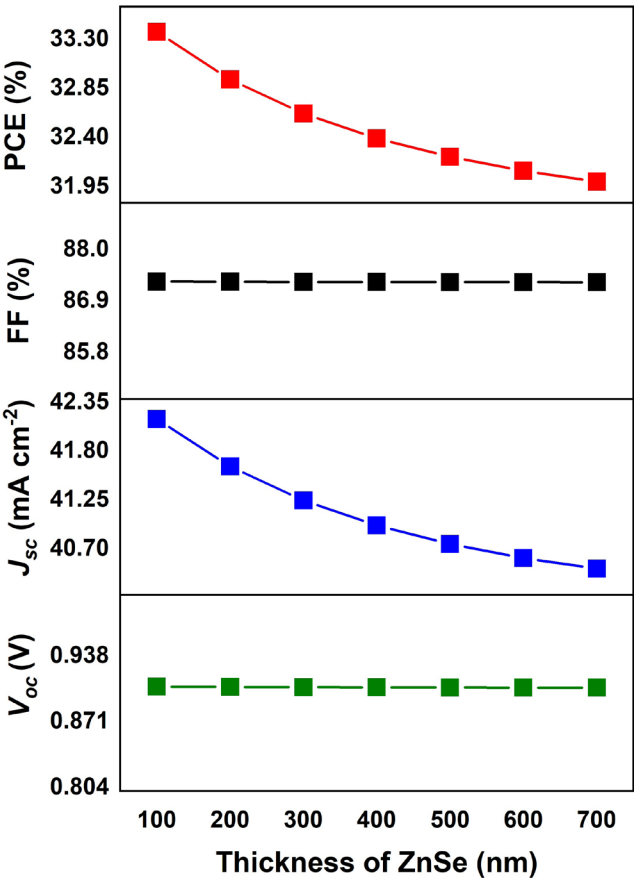

Fig. 4 The effect of ZnSe layer thickness on photovoltaic parameters

3.3 Optimization of the titanium dioxide (TiO_2) layer thickness

The analysis of photovoltaic performance in relation to the thickness of the TiO_2 layer within the Pt/p-Si/TiO_2/n-ZnSe/FTO configuration highlights its crucial role in improving solar cell efficiency. As shown in Fig. 6, the results demonstrate a steady improvement in electrical performance as the TiO_2 thickness is increased from 2 nm to 10 nm. With a minimum thickness of 2 nm, the cell achieves a PCE of 33.29%, along with V_{oc} of 0.906 V, J_{sc} of 42.168 mA cm^{-2}, and a FF of 87.15%. These values suggest effective carrier extraction; however, a thinner TiO_2 layer could lead to losses due to insufficient electric field effects or recombination at the interfaces [41].

As the thickness of TiO_2 is increased to 10 nm, a significant improvement in all electrical parameters is observed. Notably, the efficiency reaches a maximum of 33.36% at this thickness, while the FF experiences a slight increase to 87.31%. In contrast, V_{oc} and J_{sc} exhibit only minor variations, remaining fairly stable. These results suggest that a thicker TiO_2 layer enhances its role as an insulating barrier, which reduces interfacial recombination and improves the separation of charge carriers. As the thickness of TiO_2 increases, the improvements in parameters like V_{oc}, J_{sc}, and FF start to diminish. For instance, the efficiency only

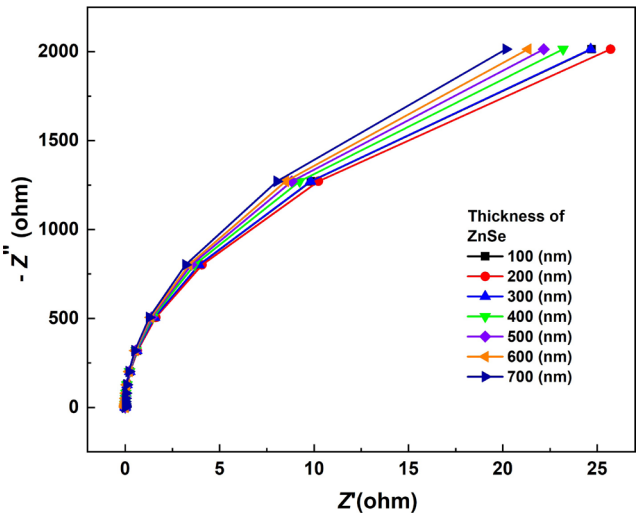

Fig. 5 Nyquist plot showing the evolution of impedance as a function of ZnSe thickness

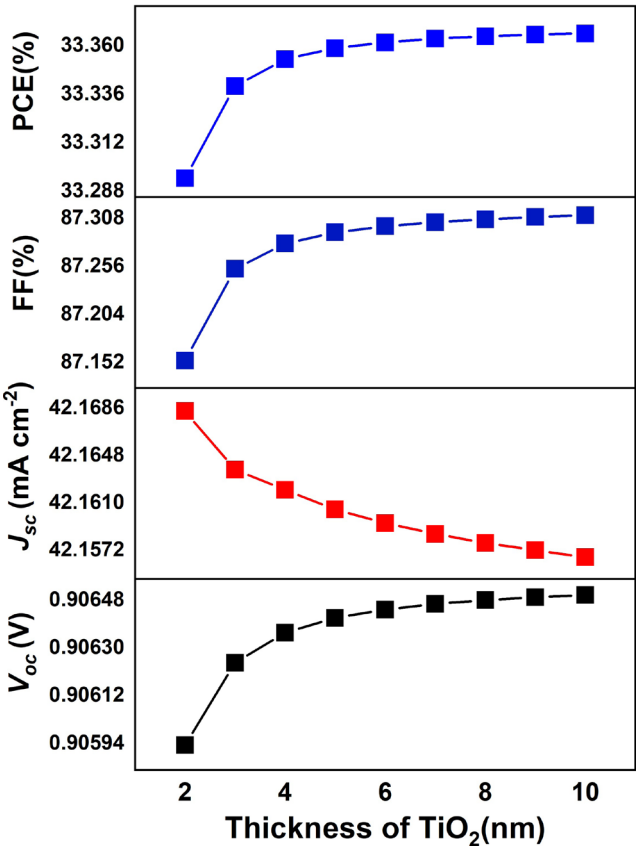

Fig. 6 The effect of TiO_2 layer thickness on photovoltaic parameters

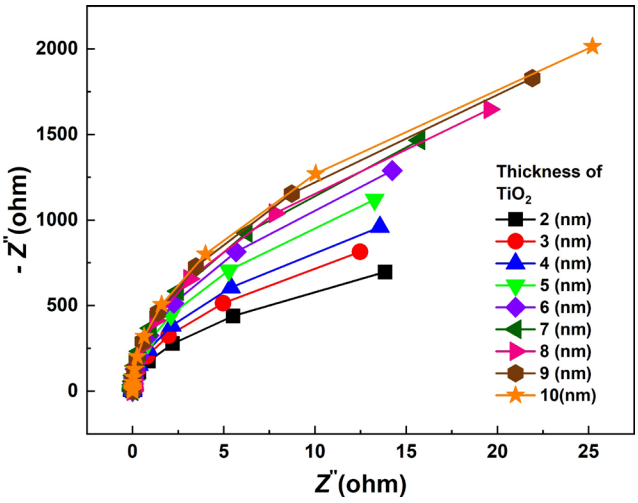

Fig. 7 Nyquist plot showing the evolution of impedance as a function of TiO_2 thickness

increases by 0.005% when comparing thicknesses of 6 nm and 10 nm, indicating that performance levels off beyond this thickness. This trend can be attributed to the fact that a thicker TiO_2 layer does not significantly improve electrical isolation or charge separation, and it may even slightly increase series resistance, which limits further enhancements in overall performance [42].

Fig. 7 displays the impedance results for different TiO_2 thicknesses. The Nyquist plots show that resistance increases as the TiO_2 thickness grows, indicating improved electrical performance attributed to better insulation [43].

A thickness of 10 nm has been determined to be optimal for the TiO_2 layer in this setup, as it improves photovoltaic efficiency by minimizing recombination losses and resistive effects. This thickness yields a V_{oc} of 0.907 V, a J_{sc} of 42.16 mA cm^{-2}, an FF of 87.31%, and a PCE of 33.37%.

3.4 Optimization of the silicon (Si) defect density

The concentration of defects in the silicon (Si) layer is crucial for the performance of SIS cells, affecting charge carrier recombination, minority carrier lifetime, and charge transport processes. Higher defect densities result in increased non-radiative recombination, which subsequently reduces both V_{oc} and J_{sc} [44]. At the Si/insulator interface, like in the case of TiO_2, these defects impede charge separation. Therefore, it is essential to keep the defect density low in order to minimize losses and improve the overall efficiency of SIS solar cells.

In this study, we examined the effects of defect density in the silicon layer, which varied from 10^{10} to 10^{18} cm^{-3}. The results are depicted in Fig. 8. At a defect density of 10^{10} cm^{-3}, the cell achieves optimal performance, with a V_{oc} of 1.03 V, a J_{sc} of 42.16 mA cm^{-2}, a FF of 86.7%, and a maximum PCE of 37.6%. However, reaching such a low defect density poses significant technological challenges due to limitations in the fabrication process and issues related to material quality.

An ideal defect density of 10^{15} cm^{-3} was identified. At this density, the photovoltaic parameters remain high, with a V_{oc} of 0.85 V, a J_{sc} of 42.12 mA cm^{-2}, an FF of 86.59%, and a conversion efficiency of 30.9%. When the defect density surpasses 10^{15} cm^{-3}, performance significantly deteriorates. At a defect density of 10^{18} cm^{-3}, the efficiency drops to 13.16%, mainly due to increased non-radiative recombination. High defect densities drastically reduce the minority carrier lifetime, which affects V_{oc} and limits the effective collection of charge carriers. Fig. 9 illustrates the recombination rates linked to different defect densities in the silicon layer. An increase in defect density leads to a marked rise in recombination at the interface, underscoring its negative impact on photovoltaic efficiency.

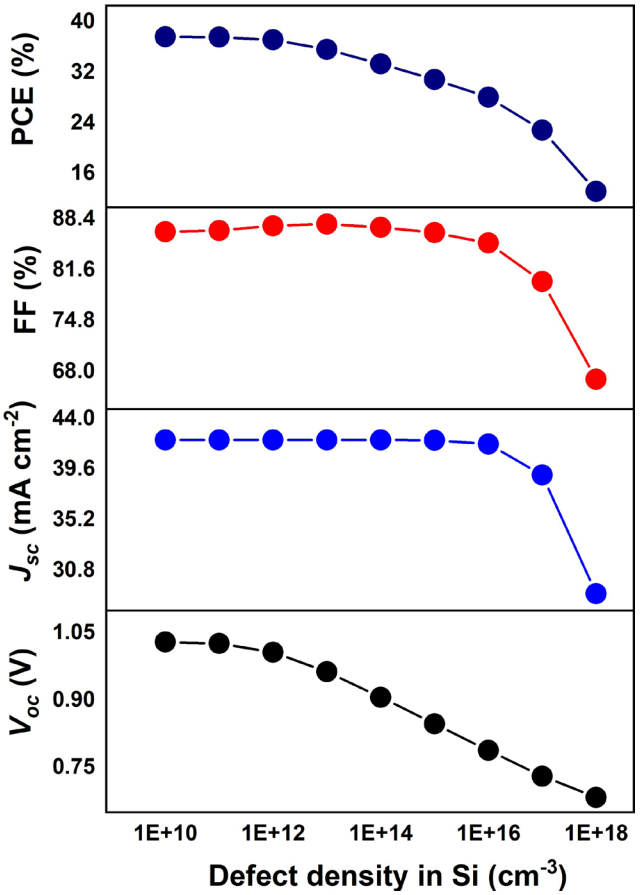

Fig. 8 The effect of silicon (Si) layer defect density on photovoltaic parameters

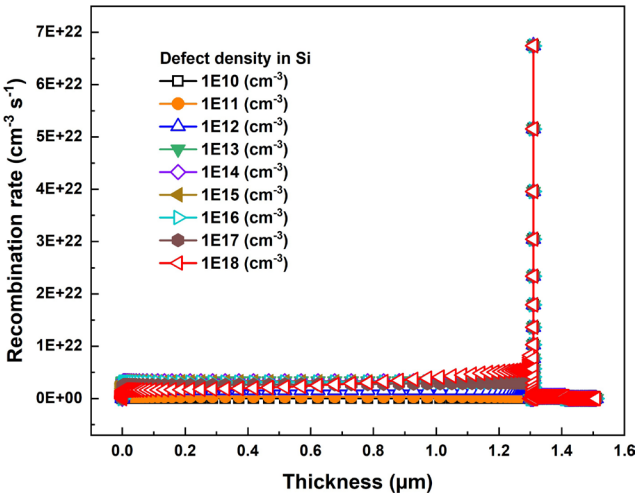

Fig. 9 Recombination rate variation with cell thickness for various defect densities in the silicon (Si) layer

3.5 Optimization of the zinc selenide (ZnSe) defect density

The concentration of defects in the ZnSe layer impacts the recombination processes, which in turn affects the overall efficiency of the solar cells. Fig. 10 illustrates the variation of photovoltaic parameters as a function of the defect density in ZnSe, ranging from 10^{10} cm^{-3} to 10^{18} cm^{-3}. The results show that photovoltaic parameters, including V_{oc}, J_{sc}, FF, and PCE, tend to remain fairly stable despite an increase in defect density. However, a slight decrease in performance is observed, particularly in open-circuit voltage and conversion efficiency, when defect density reaches high levels. This decline is associated with a rise in recombination events occurring within the active layer and at the interfaces.

Fig. 11 illustrates this increased recombination rate in areas near the interfaces at the highest defect densities. This degradation is still minimal, suggesting that the configuration under investigation, especially the ZnSe layer, demonstrates a degree of tolerance to defects [45].

The results suggest that the Pt/p-Si/TiO_2/n-ZnSe/FTO configuration exhibits consistent photovoltaic performance, even in the presence of moderate defect densities affecting material quality. This makes it a promising choice for practical applications, where achieving total defect control remains a considerable technical challenge. We have chosen a defect density of 10^{15} cm^{-3} as optimal for

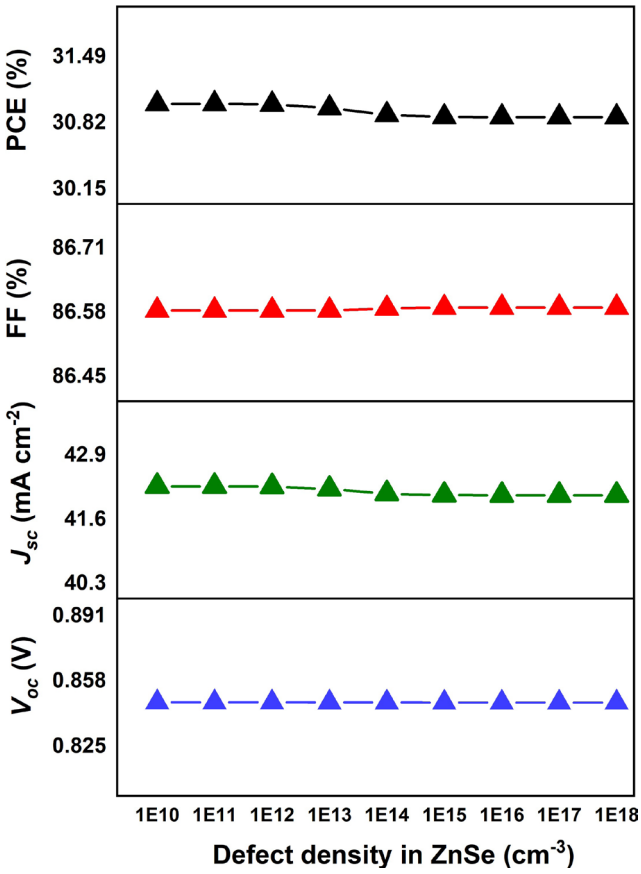

Fig. 10 The effect of ZnSe layer defect density on photovoltaic parameters

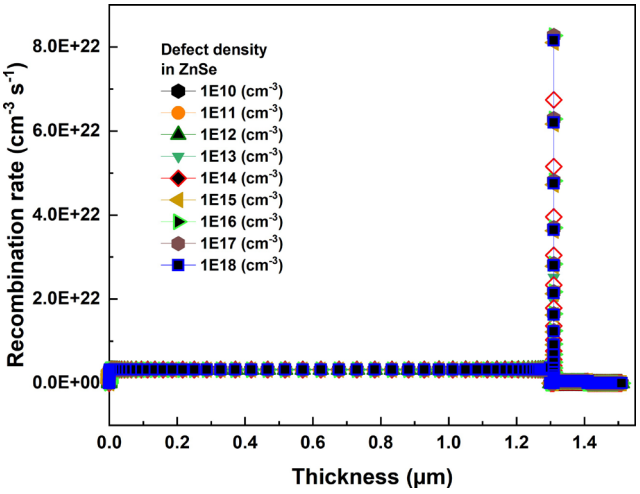

Fig. 11 Recombination rate variation with cell thickness for various defect densities in the ZnSe layer

the ZnSe layer, corresponding to a V_{oc} of 0.85 V, a J_{sc} of 42.09 mA cm^{-2}, an FF of 86.59%, and a PCE of 30.88%.

3.6 Optimization of the defect density at the Si/TiO_2 interface

Improving the interfaces in solar cell structures, especially at the Si/TiO_2 junction, is crucial for increasing the overall efficiency of the devices. In an SIS solar cell, the interactions among different layers play a key role in charge carrier transport, recombination processes, and energy conversion efficiency. Poor management of these interfaces, particularly when they have a high defect density, can lead to increased rates of electron-hole recombination, which ultimately reduces the solar cell's performance [46].

Fig. 12 illustrates the effect of defect density at the Si/TiO_2 interface on the solar cell's output parameters. When the defect density is low (10^{10} cm^{-2}), the cell achieves a PCE of 30.88%, with V_{oc} of 0.85 V, J_{sc} of 42.09 mA cm^{-2}, and a FF of 86.59%. These values indicate a comparatively low rate of charge carrier recombination, which enhances the collection and extraction of charges generated by illumination.

However, as the defect density increases (from 10^{12} cm^{-2} to 10^{16} cm^{-2}), a slight decline in performance is observed. Although V_{oc} remains relatively high (around 0.84 V), it begins to decrease with higher defect densities. This decrease can be attributed to increased carrier recombination at the Si/TiO_2 interface, which reduces the cell's ability to sustain a high voltage. Although the short-circuit current density remains stable across this range of defect density, there is a minor decline in the FF, indicating a decrease in the efficiency of charge extraction.

When the defect density reaches very high values, such as 10^{18} cm^{-2}, the solar cell's performance drops

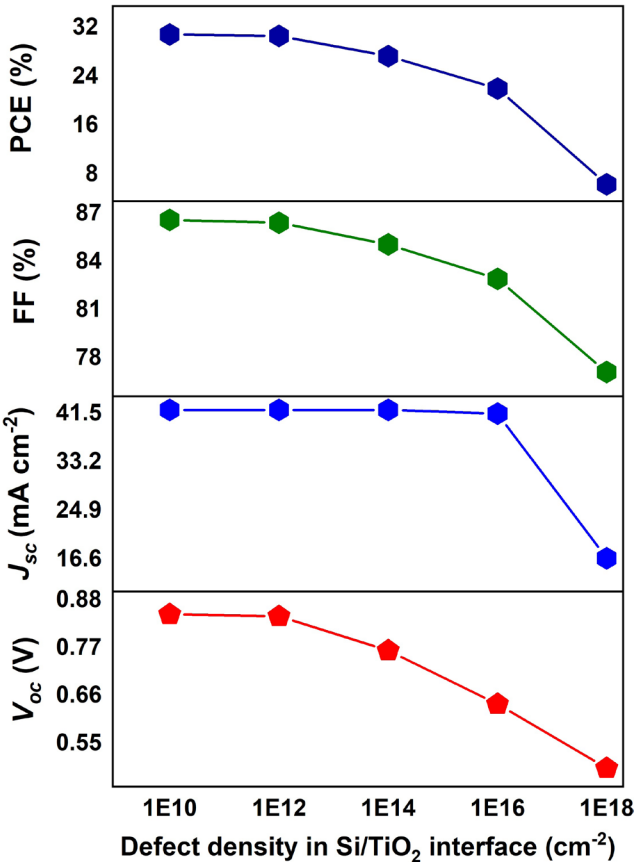

Fig. 12 The effect of Si/TiO_2 interface defect density on photovoltaic parameters

significantly. V_{oc} declines sharply, reaching only 0.5 V, while J_{sc} decreases to 16.74 mA cm^{-2}. The reduction is due to significant electron-hole recombination happening at the interface, which reduces the collection of charge carriers. Consequently, the FF drops to 77.12%, resulting in an overall cell efficiency of 6.36%, reflecting a significant decline in performance.

To better understand the effect of defect density on SIS cell performance, we plotted the conduction and valence bands as a function of the device thickness Fig. 13. These bands reveal how the energy potential is affected by variations in defect density at the Si/TiO_2 interface. At a low defect density (10^{10} cm^{-2}), the bands exhibit a regular and continuous distribution, facilitating efficient charge carrier transport. As defect density increases, the bands progressively flatten. This flattening signifies an increase in trap states, which impedes the separation and movement of charge carriers. As a result, there is a gradual decrease in both V_{oc} and FF. At extremely high defect density levels (10^{18} cm^{-2}), the band flattening becomes pronounced, resulting in a significant reduction in J_{sc} and, consequently, a drastic decline in the cell's overall efficiency.

Based on our analysis, we selected a defect density of 10^{12} cm^{-2} as optimal for the Si/TiO_2 interface. The

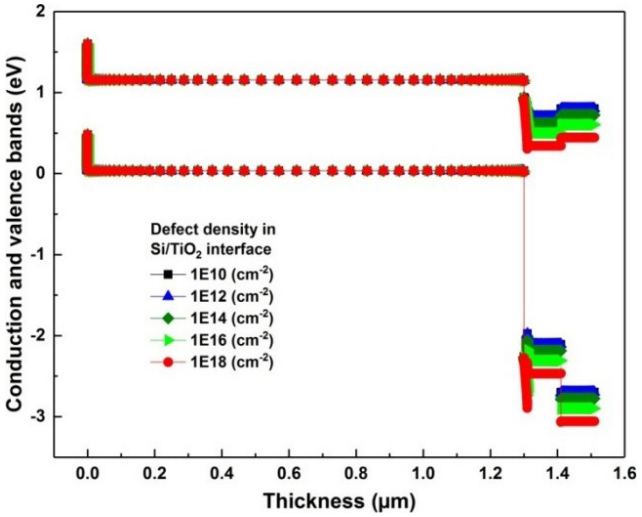

Fig. 13 Diagram of conduction and valence bands for different defect densities at the Si/TiO_2 interface as a function of cell position

corresponding parameters for this defect density are a V_{oc} of 0.85 V, a J_{sc} of 42.09 mA cm^{-2}, an FF of 86.42%, and a PCE of 30.65%.

3.7 Optimization of the defect density at the TiO_2/ZnSe interface

Inside SIS solar cell, the TiO_2/ZnSe interface plays a significant role in the transport and separation of charge carriers. Unlike the Si/TiO_2 interface, the cell's performance remains remarkably stable with variations in defect density at this interface, as shown in Fig. 14. Output parameters such as V_{oc}, J_{sc}, FF, and PCE exhibit negligible changes even when the defect density at the TiO_2/ZnSe interface varies from 10^{10} cm^{-2} to 10^{18} cm^{-2}.

At a defect density of 10^{10} cm^{-2}, the cell achieves a V_{oc} of 0.842 V, a J_{sc} of 42.094 mA cm^{-2}, an FF of 86.419%, and a PCE of 30.65%. These values remain almost unchanged as the defect density increases. For example, at 10^{18} cm^{-2}, the cell exhibits similar performance, with a V_{oc} of 0.842 V, a J_{sc} of 42.090 mA cm^{-2}, an FF of 86.419%, and a PCE of 30.64%. These results indicate that the TiO_2/ZnSe interface demonstrates high resilience to variations in defect density, in contrast to the Si/TiO_2 interface, which is more sensitive.

To enhance the understanding of this phenomenon, the conduction and valence bands were plotted against the device thickness, as illustrated in Fig. 15. Unlike the Si/TiO_2 interface, the conduction and valence bands at the TiO_2/ZnSe interface demonstrate significant stability, regardless of defect density. This stability indicates that defects have little impact on the transport of charge carriers at this interface. Additionally, it underscores the

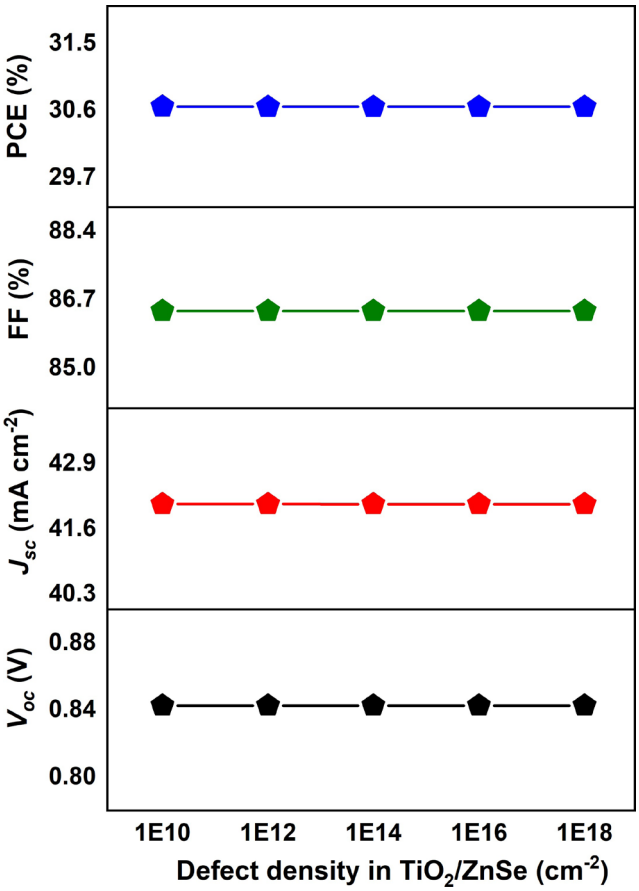

Fig. 14 The Effect of TiO_2/ZnSe interface defect density on photovoltaic parameters

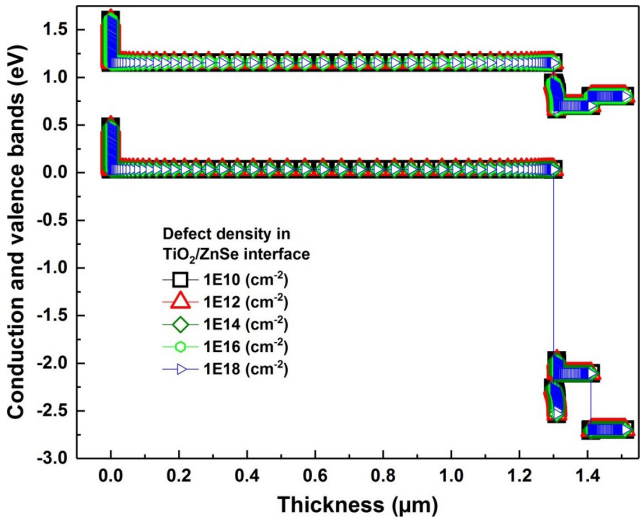

Fig. 15 Diagram of conduction and valence bands for different defect densities at the TiO_2/ZnSe interface as a function of cell position

effective control of trap states, ensuring that the cell's performance remains unaffected by significant variations in defect density [47].

The impressive stability of the TiO_2/ZnSe interface, even with variations in defect density, means that the overall performance of the cell remains largely unchanged by this factor. This reliable behavior contributes to the durability and reliability of SIS solar cells, particularly in environments where manufacturing or operational conditions may introduce defects at this interface. Based on our analysis, we selected a defect density of 10^{12} cm^{-2} as optimal for the TiO_2/ZnSe interface. The corresponding parameters for this defect density are a V_{oc} of 0.84 V, a J_{sc} of 42.09 mA cm^{-2}, an FF of 86.42%, and a PCE of 30.65%.

3.8 Optimization of the defect density at the ZnSe/FTO interface

The ZnSe/FTO interface is essential for the movement of charge carriers produced within the SIS cell. Like the TiO_2/ZnSe interface, the findings indicate that the cell's overall performance remains significantly stable, despite fluctuations in defect density at the ZnSe/FTO interface, which varies from 10^{10} to 10^{18} cm^{-2}, as illustrated in Fig. 16.

The output parameters of the cell show minimal variation across the specified range of defect densities. At a defect density of 10^{10} cm^{-2}, the cell achieves a V_{oc} of 0.842 V, a J_{sc} of 42.092 mA cm^{-2}, a FF of 86.419%, and a PCE of 30.648%. These performance metrics remain largely consistent as the defect density increases. At a defect density of 10^{18} cm^{-2}, the recorded parameters are a V_{oc} of 0.842 V, a J_{sc} of 42.090 mA cm^{-2}, an FF of 86.419%, and a PCE of 30.647%.

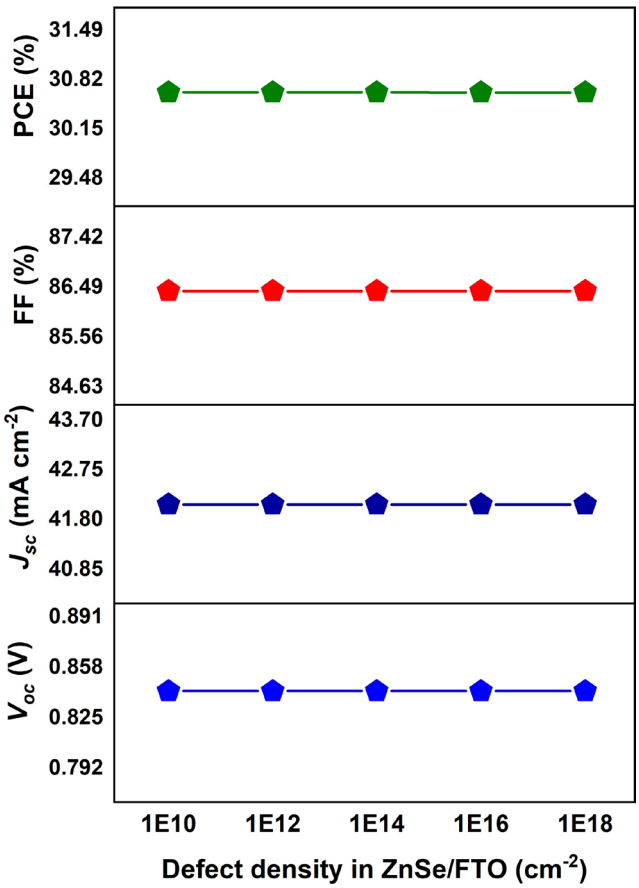

Fig. 16 The effect of ZnSe/FTO interface defect density on photovoltaic parameters

This exceptional stability can be attributed to the limited impact of ZnSe/FTO interface defects on the recombination of charge carriers. In contrast to other interfaces, like Si/TiO_2, this particular interface seems to be effectively controlled regarding traps and recombination processes, which guarantees reliable performance even in the presence of fluctuating defect states. The conduction and valence bands shown in Fig. 17 support this observation.

They exhibit a consistent and stable nature, remaining unchanged by the defect density at the ZnSe/FTO interface. This indicates that there are no major disruptions in charge carrier transport in this area.

The ZnSe/FTO interface demonstrates remarkable stability despite variations in defect density, which helps maintain consistent performance of the cell. This stability provides considerable benefits for SIS cells, improving their reliability in scenarios where defect density might change during manufacturing or operation. We have chosen a defect density of 10^{12} cm^{-2} as optimal for the ZnSe/FTO interface. The parameters corresponding to this value are a V_{oc} of 0.84 V, a J_{sc} of 42.09 mA cm^{-2}, an FF of 86.42%, and a PCE of 30.65%.

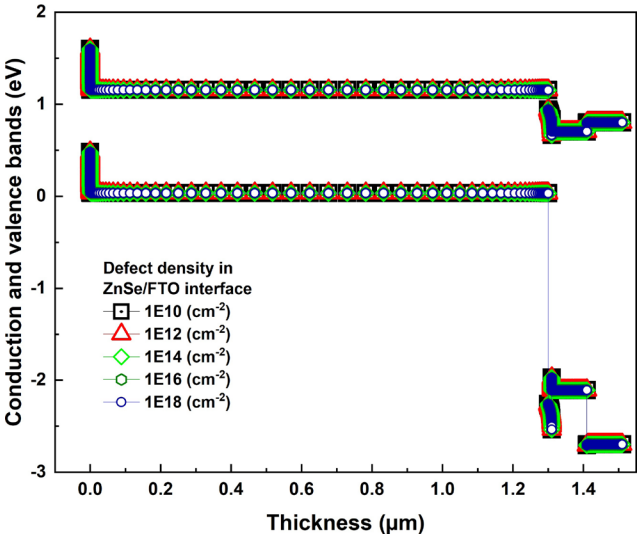

Fig. 17 Diagram of conduction and valence bands for different defect densities at the ZnSe/FTO interface as a function of cell position

3.9 Influence of temperature on device performance

Temperature plays a vital role in the efficiency of solar cells, as it directly affects the movement of charge carriers, the rates of recombination, and associated thermal losses [48]. We investigated how temperature fluctuations ranging from 300 K to 440 K influence the output characteristics of the SIS cell, specifically focusing on V_{oc}, J_{sc}, FF, and PCE, as illustrated in Fig. 18.

At a standard ambient temperature of 300 K, the cell demonstrates peak performance, achieving a V_{oc} of 0.84 V, a J_{sc} of 42.09 mA cm^{-2}, an FF of 86.42%, and a PCE of 30.65%. However, as the temperature rises, there is a notable decrease in V_{oc}, FF, and the overall efficiency of the cell, while J_{sc} remains relatively stable with a slight increase. The reduction in V_{oc} with increasing temperature is mainly due to the decrease in the energy bandgap (E_g) of the active materials, which leads to an increase in the reverse saturation current (J_{sc}) and subsequently lowers the open-circuit voltage [49].

At a temperature of 440 K, V_{oc} decreases to 0.67 V, representing a decline of about 20.6% from its original value at 300 K. Conversely, J_{sc} experiences a modest rise with increasing temperature, increasing from 42.092 mA cm^{-2} to 42.421 mA cm^{-2} as the temperature transitions from 300 K to 440 K. This slight enhancement is likely due to better charge carrier generation at elevated temperatures, although the change is not substantial.

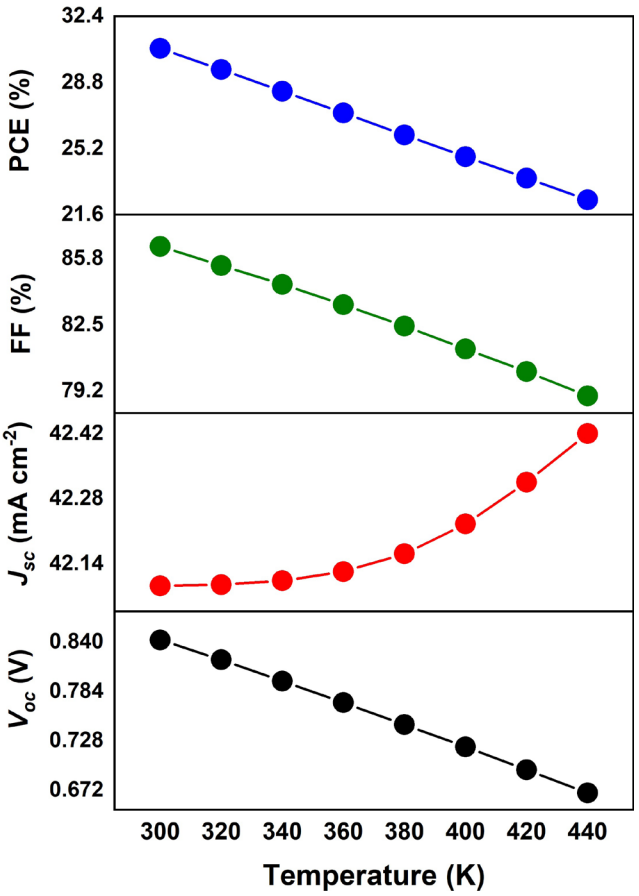

Fig. 18 Effect of temperature on photovoltaic parameters

The FF decreases with increasing temperature, decreasing from 86.42% to 78.96%. This decline indicates a deterioration in charge carrier extraction and a rise in ohmic losses within the cell. While the overall PCE experiences a notable reduction with increasing temperature, it still exceeds 22% at 440 K, showcasing the SIS cell's remarkable thermal stability. This feature is especially advantageous for use in high-temperature settings. Raising the temperature results in a gradual decline in V_{oc}, FF, and overall cell efficiency, even though there is a minor rise in J_{sc}. Nevertheless, the cell's capacity to sustain efficiency exceeding 22% under severe thermal conditions underscores its exceptional thermal stability, which is a significant advantage for consistent performance in challenging environments.

4 Conclusion

In this study, we developed and optimized a new SIS solar cell architecture using SCAPS-1D simulation software [27] to improve its efficiency. By optimizing several critical parameters such as layer thickness, defect densities, interface defect densities, and temperature, we successfully attained exceptional performance. The improved Pt/Si/TiO_2/ZnSe/FTO setup achieved a V_{oc} of 0.84 V, a J_{sc} of 42.09 mA cm^{-2}, a FF of 86.42%, and a PCE of 30.65%. The results were achieved under standard testing conditions (AM1.5G, at a temperature of 300 K). The optimized parameters consist of a Si layer thickness of 1300 nm, a ZnSe layer thickness of 100 nm, and an insulating TiO_2 layer thickness of 10 nm. Additionally, a defect density of 10^{15} cm^{-3} was chosen for the Si and ZnSe layers, while the defect density at the interfaces was optimized to 10^{12} cm^{-3}. The modifications made led to a notable enhancement in the efficiency of the cells, especially through the reduction of charge recombination and the optimization of charge transport. This research offers essential parameters for the future advancement of SIS solar cells and sets the stage for experimental efforts aimed at validating these improvements. Additionally, it underscores the significance of refining material properties and the design of solar cells to achieve superior performance and further the progress of solar technology.

Funding
The authors declare that no funds, grants, or other supports were received during the preparation of this manuscript.

Data availability
All data generated or analyzed during this study are included in this manuscript.

Conflict of interest
The authors have no relevant financial or non-financial interests to disclose.

Acknowledgement
The work is included in the PRFU project under contract number B00L02UN310220220002 at University of Science and Technology of Oran Mohamed-Boudiaf (USTOMB).

References

[1] Luan, J., Zhang, Y., Ma, N., Tian, J., Li, X., Liu, D. "Evaluating the uncertainty of eight approaches for separating the impacts of climate change and human activities on streamflow", Journal of Hydrology, 601, 126605, 2021. https://doi.org/10.1016/j.jhydrol.2021.126605

[2] Tang, Y. H., Luan, X. B., Sun, J. X., Zhao, J. F., Yin, Y. L., Wang, Y. B., Sun, S. K. "Impact assessment of climate change and human activities on GHG emissions and agricultural water use", Agricultural and Forest Meteorology, 296, 108218, 2021. https://doi.org/10.1016/j.agrformet.2020.108218

[3] Ahmad, T., Zhang, D. "A critical review of comparative global historical energy consumption and future demand: The story told so far", Energy Reports, 6, pp. 1973–1991, 2020. https://doi.org/10.1016/j.egyr.2020.07.020

[4] Kaka, F., Keshav, M., Ramamurthy, P. C. "Optimising the photovoltaic parameters in donor–acceptor–acceptor ternary polymer solar cells using machine learning framework", Solar Energy, 231, pp. 447–457, 2022. https://doi.org/10.1016/j.solener.2021.11.054

[5] Nikolaidis, P., Poullikkas, A. "Increasing the Photovoltaic Hosting Capacity in Autonomous Grids and Microgrids via Enhanced Priority-List Schemes and Storage", Green Energy and Sustainability, 1(1), 0002, 2021. https://doi.org/10.47248/HKOD902101010002

[6] Fritts, C. E. "On a New form of Selenium Cell, and Some Electrical Discoveries made by its use", American Journal of Science, S3-26(156), pp. 465–472, 1883. https://doi.org/10.2475/ajs.s3-26.156.465

[7] Shewchun, J., Singh, R., Green, M. A. "Theory of metal-insulator-semiconductor solar cells", Journal of Applied Physics, 48(2), pp. 765–770, 1977. https://doi.org/10.1063/1.323667

[8] Fonash, S. J. "Outline and comparison of the possible effects present in a metal–thin–film–insulator–semiconductor", Journal of Applied Physics, 47(8), pp. 3597–3602, 1976. https://doi.org/10.1063/1.323164

[9] Shewchun, J., Dubow, J., Wilmsen, C. W., Singh, R., Burk, D., Wager, J. F. "The operation of the semiconductor-insulator-semiconductor solar cell: Experiment", Journal of Applied Physics, 50(4), pp. 2832–2839, 1979. https://doi.org/10.1063/1.326196

[10] Bethge, O., Nobile, M., Abermann, S., Glaser, M., Bertagnolli, E. "ALD grown bilayer junction of ZnO:Al and tunnel oxide barrier for SIS solar cell", Solar Energy Materials and Solar Cells, 117, pp. 178–182, 2013. https://doi.org/10.1016/j.solmat.2013.04.028

[11] Kobayashi, H., Ishida, T., Nakato, Y., Tsubomura, H. "Mechanism of carrier transport in highly efficient solar cells having indium tin oxide/Si junctions", Journal of Applied Physics, 69(3), pp. 1736–1743, 1991. https://doi.org/10.1063/1.347220

[12] Dasgupta, K., Mondal, A., Ray, S., Gangopadhyay, U. "Mathematical Modelling of a Novel Hetero-junction Dual SIS ZnO-Si-SnO Solar Cell", 14(7), pp. 3329–3338, 2022. https://doi.org/10.1007/s12633-021-01090-8

[13] Salah, H. Y., Abdelfatah, M., El-Shaer, A., Oraby, A. H. "Effect of Al doped ZnO on optical and photovoltaic properties of the p-Cu_2O/n-AZO solar cells", Ceramics International, 49(5), pp. 7746–7752, 2023. https://doi.org/10.1016/j.ceramint.2022.10.277

[14] Salah, H. Y., Bakry, M., Kubas, M., Ismail, W., El-Henawey, M. I., Oraby, A. H., El-Shaer, A., Abdelfatah, M. "Improvement of the structural, morphological, optical, and photoelectrochemical properties of Al-doped ZnO nanorods for use in biosensors and solar cells", The European Physical Journal Plus, 137(12), 1319, 2022. https://doi.org/10.1140/epjp/s13360-022-03532-7

[15] Dasgupta, K., Bose, S., Mondal, A., Jana, S., Gangopadhyay, U. "Fabrication and Mathematical Modelling of a ITO-Al_2O_3-Si SIS Solar Cell", Silicon, 14(17), pp. 11963–11977, 2022. https://doi.org/10.1007/s12633-022-01910-5

[16] Shameli, M. A., Mirnaziry, S. R., Yousefi, L. "A Thin-Film SIS Solar Cell Based on Distributed Silicon Nanoparticles", In: 2021 29th Iranian Conference on Electrical Engineering (ICEE), Tehran, Iran, 2021, pp. 816–820. ISBN 978-1-6654-3366-2 https://doi.org/10.1109/ICEE52715.2021.9544423

[17] Qiao, Z., Zhang, M., Wu, B., Zhang, T., Ruan, Y., Chen, J., Huang, L., Wu, J., Qi, Y., Yang, X. "Inorganic tin-based perovskite solar cells: Modeling and performance analysis of hole transport layer-free structures", Chemical Physics Letters, 813, 140295, 2023. https://doi.org/10.1016/j.cplett.2022.140295

[18] Bodurov, G., Ivanova, T., Gesheva, K. "Technology and application of transition metal oxide of WVO as functional layers and NiO thin films as counter electrode material in electrochromic "Smart Windows"", Physics Procedia, 46, pp. 149–158, 2013. https://doi.org/10.1016/j.phpro.2013.07.057

[19] Pavan, M., Rühle, S., Ginsburg, A., Keller, D. A., Barad, H.-N., Sberna, P. M., …, Fortunato, E. "TiO_2/Cu_2O all-oxide heterojunction solar cells produced by spray pyrolysis", Solar Energy Materials and Solar Cells, 132, pp. 549–556, 2015. https://doi.org/10.1016/j.solmat.2014.10.005

[20] Jose, R., Thavasi, V., Ramakrishna, S. "Metal oxides for dye-sensitized solar cells", Journal of the American Ceramic Society, 92(2), pp. 289–301, 2009. https://doi.org/10.1111/j.1551-2916.2008.02870.x

[21] Laidouci, A., Mamta, Singh, V. N., Dakua, P. K., Panda, D. K. "Performance evaluation of $ZnSnN_2$ solar cells with Si back surface field using SCAPS-1D: A theoretical study", Heliyon, 9(10), e20601, 2023. https://doi.org/10.1016/j.heliyon.2023.e20601

[22] Roy, A., Benhaliliba, M. "Investigation of ZnO/p-Si heterojunction solar cell: Showcasing experimental and simulation study", Optik, 274, 170557, 2023. https://doi.org/10.1016/j.ijleo.2023.170557

[23] Ijaz, S., Raza, E., Ahmad, Z., Zubair, M., Mehmood, M. Q., Mehmood, H., Massoud, Y., Rehman, M. M. "Numerical simulation to optimize the efficiency of HTM-free perovskite solar cells by ETM engineering", Solar Energy, 250, pp. 108–118, 2023. https://doi.org/10.1016/j.solener.2022.12.027

[24] Dris, K., Benhaliliba, M., Ayeshamariam, A., Roy, A., Kaviyarasu, K. "Improving the perovskite solar cell by insertion of methyl ammonium tin oxide and cesium tin chloride as absorber layers: scaps 1d study based on experimental studies", Journal of Optics, 2024. https://doi.org/10.1007/s12596-024-01996-7

[25] Dris, K., Benhaliliba, M. "Study and Optimization of a New Perovskite Solar Cell Structure Based on the Two Absorber Materials Cs2TiBr6 and MASnBr3 Using SCAPS 1D", Periodica Polytechnica Chemical Engineering, 68(3), pp. 348–363, 2024. https://doi.org/10.3311/PPch.36825

[26] El-Naggar, A. A., Lotfy, L. A., Felfela, A. A., Ismail, W., Abdelfatah, M., Sharshir, S. W., El-Shaer, A. "Numerical simulation-based performance enhancement approach for an inorganic $BaZrS_3$/CuO heterojunction solar cell", Scientific Reports, 14(1), 7614, 2024. https://doi.org/10.1038/s41598-024-57636-4

[27] Burgelman, M., University of Gent "SCAPS: Solar Cell Capacitance Simulator, (3.3.10)", [computer program] Available at: http://scaps.elis.ugent.be/ [Accessed: 30 April 2021]

[28] Saikia, D., Bera, J., Betal, A., Sahu, S. "Performance evaluation of an all inorganic $CsGeI_3$ based perovskite solar cell by numerical simulation", Optical Materials, 123, 111839, 2022. https://doi.org/10.1016/j.optmat.2021.111839

[29] Merzougui, L., Benhaliliba, M., Ayeshamariam, A. "Enhancing the performance of AZO/ZnO-i/CdS/CSTS hybrid solar cell by incorporating an ultra-thin P3HT layer: a combined simulation and impedance spectroscopy study using experimental results", Journal of Optics, 2024. https://doi.org/10.1007/s12596-024-02324-9

[30] Dris, K., Benhaliliba, M. "Novel Inorganic–Organic Heterojunction Solar Cell-Based Perovskite Using Two Absorbent Materials", Nano, 18(11), 2350091, 2023. https://doi.org/10.1142/S1793292023500911

[31] Hossain, M. K., Rubel, M. H. K., Toki, G. F. I., Alam, I., Rahman, M. F., Bencherif, H. "Effect of Various Electron and Hole Transport Layers on the Performance of $CsPbI_3$-Based Perovskite Solar Cells: A Numerical Investigation in DFT, SCAPS-1D, and wxAMPS Frameworks", ACS Omega, 7(47), pp. 43210–43230, 2022. https://doi.org/10.1021/acsomega.2c05912

[32] Mushtaq, S., Tahir, S., Ashfaq, A., Sebastian Bonilla, R., Haneef, M., Saeed, R., Ahmad, W., Amin, N. "Performance optimization of lead-free $MASnBr_3$ based perovskite solar cells by SCAPS-1D device simulation", Solar Energy, 249, pp. 401–413, 2023. https://doi.org/10.1016/j.solener.2022.11.050

[33] Islam, M. A., Paul, R. "A lead-free inorganic Cs_2TiX_6-based heterostructure perovskite solar cell design and performance evaluation", Optical and Quantum Electronics, 55(11), 957, 2023. https://doi.org/10.1007/s11082-023-05238-1

[34] Puente-López, E., Pal, M. "Numerical simulation and optimization of physical properties for high efficiency $CuSbS_2$ thin film solar cells", Optik, 272, 170233, 2023. https://doi.org/10.1016/j.ijleo.2022.170233

[35] Bohra, S. S., Panchal, A. K. "Optimization of absorber layers' thickness in a Si micromorph solar cell for current matching with intermediate ZnO reflector", Journal of Renewable and Sustainable Energy, 5(2), 023121, 2013. https://doi.org/10.1063/1.4798319

[36] Mortadi, A.,El Hafidi, E., Monkade, M., El Moznine, R. "Investigating the influence of absorber layer thickness on the performance of perovskite solar cells: A combined simulation and impedance spectroscopy study", Materials Science for Energy Technologies, 7, pp. 158–165, 2024. https://doi.org/10.1016/j.mset.2023.10.001

[37] Souri, S., Marandi, M. "Numerical modelling of the effect of the Ag: ZnSe BSF layer on the high performance of ZnSe/CdTe thin film solar cells by SCAPS-1D software", Optical and Quantum Electronics, 55(5), 397, 2023. https://doi.org/10.1007/s11082-023-04563-9

[38] Vallisree, S., Thangavel, R., Lenka, T. R. "Theoretical investigations on enhancement of photovoltaic efficiency of nanostructured CZTS/ZnS/ZnO based solar cell device", Journal of Materials Science: Materials in Electronics, 29(9), pp. 7262–7272, 2018. https://doi.org/10.1007/s10854-018-8715-y

[39] Mohottige, R. N., Kalawila Vithanage, S. P. "Numerical simulation of a new device architecture for CIGS-based thin-film solar cells using 1D-SCAPS simulator", Journal of Photochemistry and Photobiology A: Chemistry, 407, 113079, 2021. https://doi.org/10.1016/j.jphotochem.2020.113079

[40] von Roos, O., Landsberg, P. T. "Effect of recombination on the open-circuit voltage of a silicon solar cell", Journal of Applied Physics, 57(10), pp. 4746–4751, 1985. https://doi.org/10.1063/1.335339

[41] Fatima, Q., Haidry, A. A., Zhang, H., El Jery, A., Aldrdery, M. "A critical review on advancement and challenges in using TiO_2 as electron transport layer for perovskite solar cell", Materials Today Sustainability, 27, 100857, 2024. https://doi.org/10.1016/j.mtsust.2024.100857

[42] Kao, M. C., Chen, H. Z., Young, S. L., Kung, C. Y., Lin, C. C. "The effects of the thickness of TiO_2 films on the performance of dye-sensitized solar cells", Thin Solid Films, 517(17), pp. 5096–5099, 2009. https://doi.org/10.1016/j.tsf.2009.03.102

[43] Elsaeedy, H. I.,Qasem, A., Yakout, H. A., Mahmoud, M. "The pivotal role of TiO_2 layer thickness in optimizing the performance of TiO_2/P-Si solar cell", Journal of Alloys and Compounds, 867, 159150, 2021. https://doi.org/10.1016/j.jallcom.2021.159150

[44] Attafi, D., Meftah, A., Boumaraf, R., Labed, M. "Enhancement of silicon solar cell performance by introducing selected defects in the SiO_2 passivation layer", Optik, 229, 166206, 2021. https://doi.org/10.1016/j.ijleo.2020.166206

[45] Yoon, S.-Y.,Kim, Y.-H., Lee, S.-H., Yang, H., Jo, D.-Y., Kim, H.-M., Kim, Y., Park, S. M., Choi, S. W., Yang, H. "Efficient, stable blue light-emitting diodes enabled by heterostructural alteration of ZnSeTe quantum dot and functionalization of ZnMgO", Advanced Optical Materials, 12(32), 2401085, 2024. https://doi.org/10.1002/adom.202401085

[46] Haque, M. M., Mahjabin, S., Khan, S., Hossain, M. I., Muhammad, G., Shahiduzzaman, M., Sopian, K., Akhtaruzzaman, M. "Study on the interface defects of eco-friendly perovskite solar cells", Solar Energy, 247, pp. 96–108, 2022. https://doi.org/10.1016/j.solener.2022.10.024

[47] Njema, G. G.,Kibet, J. K., Ngari, S. M. "A review of interface engineering characteristics for high performance perovskite solar cells", Measurement: Energy, 2, 100005, 2024. https://doi.org/10.1016/j.meaene.2024.100005

[48] Mortadi, A.,Tabbai, Y., El Hafidi, E., Nasrellah, H., Chahid, E., Monkade, M., El Moznine, R. "Investigating temperature effects on perovskite solar cell performance via SCAPS-1D and impedance spectroscopy", Cleaner Engineering and Technology, 24, 100876, 2025. https://doi.org/10.1016/j.clet.2024.100876

[49] Löper, P., Pysch, D., Richter, A., Hermle, M., Janz, S., Zacharias, M. Glunz, S. W. "Analysis of the temperature dependence of the open-circuit voltage", Energy Procedia, 27, pp. 135–142, 2012. https://doi.org/10.1016/j.egypro.2012.07.041